Water's second glass transition

Katrin Amann-Winkel[a,1], Catalin Gainaru[b,1], Philip H. Handle[a], Markus Seidl[a], Helge Nelson[b], Roland Böhmer[b], and Thomas Loerting[a]

[a]Institute of Physical Chemistry, University of Innsbruck, A-6020 Innsbruck, Austria; and [b]Fakultät Physik, Technische Universität Dortmund, D-44221 Dortmund, Germany

Edited by Pablo G. Debenedetti, Princeton University, Princeton, NJ, and approved September 19, 2013 (received for review June 19, 2013)

The glassy states of water are of common interest as the majority of H_2O in space is in the glassy state and especially because a proper description of this phenomenon is considered to be the key to our understanding why liquid water shows exceptional properties, different from all other liquids. The occurrence of water's calorimetric glass transition of low-density amorphous ice at 136 K has been discussed controversially for many years because its calorimetric signature is very feeble. Here, we report that high-density amorphous ice at ambient pressure shows a distinct calorimetric glass transitions at 116 K and present evidence that this second glass transition involves liquid-like translational mobility of water molecules. This "double T_g scenario" is related to the coexistence of two liquid phases. The calorimetric signature of the second glass transition is much less feeble, with a heat capacity increase at $T_{g,2}$ about five times as large as at $T_{g,1}$. By using broadband-dielectric spectroscopy we resolve loss peaks yielding relaxation times near 100 s at 126 K for low-density amorphous ice and at 110 K for high-density amorphous ice as signatures of these two distinct glass transitions. Temperature-dependent dielectric data and heating-rate–dependent calorimetric data allow us to construct the relaxation map for the two distinct phases of water and to extract fragility indices m = 14 for the low-density and m = 20–25 for the high-density liquid. Thus, low-density liquid is classified as the strongest of all liquids known ("superstrong"), and also high-density liquid is classified as a strong liquid.

supercooled water | polyamorphism | differential scanning calorimetry | dielectric relaxation

In space, solid water is predominantly in the amorphous state (1, 2) and has been identified as the frost on interstellar dust grains (3), whereas on Earth it always appears as crystalline, hexagonal ice. The occurrence of water's ambient pressure glass transition at $T_{g,1} = 136 \pm 2$ K (4–6) has been discussed controversially for almost five decades mainly because its calorimetric signature is very feeble (7). Even though the question about the nature of this transition has not been settled ultimately, recent work interprets this signature to be consistent with a glass-to-liquid transition and places deeply supercooled water into the category of "strong" liquids (8–11). Lately, it has become clear that water's high-density phase exhibits a glass transition at pressures ≥0.1 GPa, which has also been interpreted in terms of a glass-to-liquid transition (12–15). However, it has remained unclear in experiments whether or not the high-pressure glass transition connects to the ambient pressure glass transition or whether water shows two distinct glass transitions at a given pressure. The latter scenario is a prerequisite for the possibility of two distinct supercooled liquid phases of water and the postulated liquid–liquid transition (16, 17), which presumably holds the key to understanding the highly anomalous nature of water (18). These two scenarios are sketched in Fig. 1 on the basis of published experimental T_g data for water up to 0.3 GPa (black symbols in Fig. 1) (4–6, 14) and recent simulations indicating a decrease in $T_{g,1}$ with pressure (dotted line in Fig. 1*B*) (17). Mishima, for instance, has linearly extrapolated T_g data collected at 0.1–0.8 GPa to ambient pressure for salty and emulsified high-density amorphous ice (HDA) samples with the result that his extrapolated T_g is about the same as the $T_{g,1} = 136 \pm 2$ K measured for low-density amorphous ice (LDA) at ambient pressure (12), which hints at the single T_g scenario depicted in Fig. 1*A*.

In the laboratory, noncrystalline ices have been prepared using various techniques such as water vapor deposition, hyperquenching of μm-sized water droplets, pressure-induced amorphization, radiation-induced vitrification, and amorphous–amorphous transitions (19). All variants of amorphous ice can be conserved in liquid nitrogen and predominantly crystallize at ambient pressure above about 150 K to cubic ice. Although amorphous ices of densities <0.95 g/cm^3 crystallize directly, the HDAs of densities >1.12 g/cm^3 studied so far experience a sharp transformation to LDA before crystallization at ambient pressure. The transformation temperature from pressure-amorphized HDA to LDA strongly depends on the sample history and varies between ∼105 K (20) and ∼133 K (21). HDA obtained by vapor deposition on substrates at <20 K even transforms at 38–68 K to LDA (22). As pointed out by Nelmes et al. this difference in thermal stability reflects the degree of relaxation (23), with pressure annealing at ∼0.1 GPa significantly enhancing thermal stability at ambient pressure (24). Work on HDA, including calorimetry studies (20), was traditionally carried out using unannealed (uHDA) samples prepared by pressure-induced amorphization of hexagonal ice at 77 K (25), whereas the study of annealed, expanded forms of HDA (eHDA) has only begun in recent years (14, 21, 23, 24). Here we present differential scanning calorimetry (DSC) experiments (Fig. 2) and dielectric relaxation spectra (Fig. 3) of eHDA samples of highest known thermal stability, prepared by slowly decompressing HDA samples at 140 K to 0.07 GPa (24). These samples allow us to detect water's second glass transition at $T_{g,2} = 116 \pm 2$ K at ambient pressure (open circle in Fig. 1*B*) in a temperature window heretofore hidden by the (premature) transition of uHDA to LDA. Consequently, the

Significance

Water is not only the most important liquid for life on Earth, but also one of the most anomalous liquids. These anomalies become most evident in the supercooled state at subzero temperatures. We show from dielectric and calorimetric studies that water in the deeply supercooled regime, below –120 °C, can even exist as two distinct, ultraviscous liquids at ambient pressure, a low- (LDL, 0.92 g/cm^3) and high-density liquid (HDL, 1.15 g/cm^3), which can both remain in the metastable, equilibrium liquid state for many hours above their calorimetric glass transition temperatures of –137 °C (136 K) and –157 °C (116 K). LDL is identified as the strongest of all liquids, and also HDL is a strong liquid at record low temperature.

Author contributions: K.A.-W., C.G., R.B., and T.L. designed research; K.A.-W., C.G., P.H.H., M.S., and H.N. performed research; K.A.-W., C.G., P.H.H., M.S., H.N., R.B., and T.L. analyzed data; and K.A.-W., C.G., R.B., and T.L. wrote the paper.

The authors declare no conflict of interest.

This article is a PNAS Direct Submission.

[1]To whom correspondence may be addressed. E-mail: katrin.winkel@uibk.ac.at or catalin.gainaru@uni-dortmund.de.

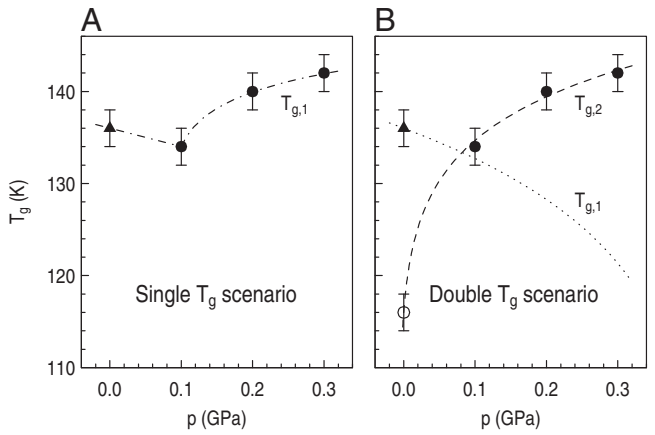

Fig. 1. Two possible scenarios to explain the metastable phase behavior of deeply supercooled water based on experimental literature T_g data for LDA (filled black triangle) (4–6) and HDA (filled black circles) (14) and compared with glass transition temperatures from computer simulations (lines) (17). The single T_g scenario, in *A* indicated by the dash-dotted line, is qualitatively similar to the situation found in water simulations using the SPC/E model (17), whereas the double T_g scenario in *B* is qualitatively similar to the situation found for the ST2 model (17). The dashed line corresponds to the $T_{g,2}$ line for HDA, whereas the dotted line corresponds to the predicted $T_{g,1}$ line for LDA. The observation of a second T_g (open circle) at ambient pressure reported in this work rules out the possibility of a single T_g scenario.

second glass transition was inaccessible in earlier studies on uHDA (19, 20). The glass transition of eHDA is by about 20 K lower than the value extrapolated by Mishima (12) and clearly distinct from LDA's glass transition at $T_{g,1} = 136 \pm 2$ K (4–6). That is, the assumption of a single T_g scenario is unsustainable, but instead a double T_g scenario is indicated from our work.

Results

Calorimetric Measurements. So far HDA is believed to always experience a solid–solid transformation directly to LDA at 1 bar, which is indeed the case for uHDA samples. However, for eHDA samples, we here observe another transition that precedes the transformation to LDA. The enthalpy relaxation exotherm, reported to occur for pressure-amorphized uHDA (20), gradually disappears with progressing annealing, and concurrently the thermal stability increases (21). At the highest known level of relaxation, the DSC scan of eHDA (Fig. 2, trace 1) now shows an endothermic increase—that is, an increase in heat capacity—at about 113 K. This was overlooked in earlier calorimetric studies (20) because uHDA of low thermal stability was used, whereas we study well-relaxed HDA (eHDA). This increase in heat capacity is repeatable: A reheating scan carried out after cooling from 123 K at a rate of $q = 30$ K/min again shows an increase in heat capacity, this time at about 116 K (Fig. 2, trace 2). Also, a third heating scan after prior cooling at 30 K/min shows this increase in heat capacity (Fig. 2, trace 3) at 116 K. Please note that the initial part of trace 3 in Fig. 1 is exactly matching trace 2 because the same cooling and heating rates were used for both scans (Fig. 2, *Inset*). Trace 1 differs from traces 2 and 3 because the sample had experienced a different type of thermal treatment before the first heating scan. The inset to Fig. 2 documents that the onset temperature in a heating scan at 10 K/min depends on the prior cooling rate. It shifts from 116 to 113 K when cooling at 1 K/min instead of 30 K/min, a typical signature of a glass transition. Together with the reproducible

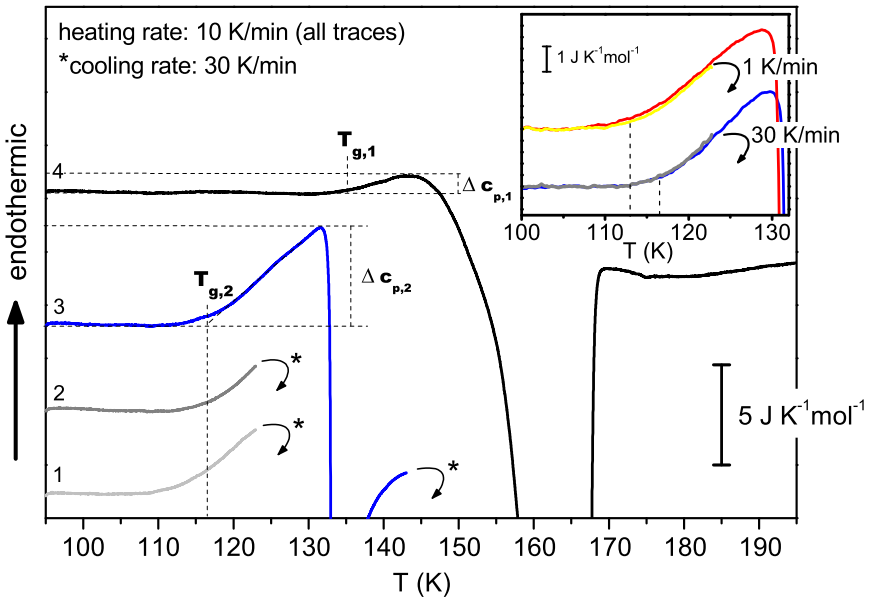

Fig. 2. DSC scans of 20.3 mg eHDA. The samples were first heated to 123 K (trace 1, light gray), followed by cooling at 30 K/min to 90 K and subsequent heating to 123 K (trace 2, dark gray), followed by cooling at 30 K/min to 90 K and subsequent heating to 145 K, at which the temperature was kept for 10 min at 145 K (trace 3, blue). The exotherm in trace 3, blue, indicates transformation to LDA. After cooling at 30 K/min to 90 K, the sample (now LDA) is heated to 253 K (trace 4, black). The exotherm in trace 4 indicates crystallization of the sample to cubic ice. The glass transition onset temperatures of LDA and eHDA are marked by $T_{g,1}$ and $T_{g,2}$, respectively, and the corresponding increase in heat capacity by $\Delta c_{p,1}$ and $\Delta c_{p,2}$. Baseline was corrected by subtracting a scan of hexagonal ice. All curves are shifted vertically for clarity. The inset shows the shift in $T_{g,2}$ in a heating scan after changing the cooling rate from 30 K/min to 1 K/min. The heating scans displayed in the inset were obtained using the same protocol. The blue and gray heating scans were measured using the protocol also used for the heating scans 2 and 3 in the main figure, whereas the red and yellow heating scans were both measured after cooling the sample 1 K/min. In the inset the blue/gray pair of traces and also the red/yellow pair are shown without vertical shift to demonstrate the exact match of two subsequent heating scans when using the same cooling/heating rate combination. The rate-dependent shift in T_g upon changing the cooling rate is a characteristic feature of the glass transition. Heating rate is always 10 K/min.

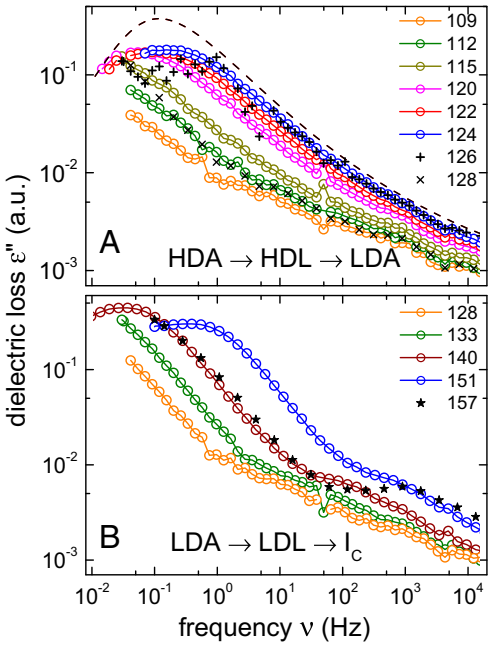

Fig. 3. Dielectric loss spectra of (*A*) HDL and (*B*) LDL are plotted as connected open symbols for several temperatures. (*A*) At 126 K the plusses reflect measurements acquired while HDL transforms to LDL. The crosses demonstrate that the relaxation in LDL is slower than in HDL. For comparison, the dielectric loss spectrum of ultraviscous glycerol (at $T = 196$ K, loss divided by 60) (44) is added (dashed line). (*B*) The transformation of LDL to cubic ice (stars) takes place above 151 K and is recognized from a shift of the spectra to lower frequencies.

increase in the heat capacity, these observations reflect the ergodicity restoration accompanied by the onset of molecular mobility and are the hallmark of a glass transition (26). This onset temperature denoted $T_{g,2}$ measured on the eHDA sample is therefore water's second glass transition temperature. Trace 3 of Fig. 2 shows that the increase in heat capacity is $\Delta c_{p,2} \sim 4.8$ $JK^{-1}{\cdot}mol^{-1}$. The value for $\Delta c_{p,2}$ represents a lower limit, as the release of latent heat for the strongly exothermic amorphous–amorphous transition from HDA to LDA that commences at ~132 K is superimposed onto the glass transition endotherm, and thus, the end point of HDA's glass transition is hidden. The apparent width of HDA's glass transition is at least ~16 K, which compares to a width of ~11 K for the glass transition observed earlier for LDA (5, 6). [The apparent width is extracted from the DSC scans as the difference in onset of exotherm and onset of glass transition, similar to the practice used in earlier studies on truncated glass transitions of LDA (e.g., ref. 27). Please note that the apparent width represents a lower limit to the true width of the glass transition. By comparison with other glass-forming liquids and aqueous solutions, in which the end point is resolved, we estimate the apparent width to be very close to the true width—that is, the glass-transition end point would occur slightly above the onset of the exotherm.] This glass transition in LDA is reproduced here (trace 4 of Fig. 2), as eHDA has converted to LDA at the end of trace 3. The heat capacity change for LDA ($\Delta c_{p,1} \sim 1$ $JK^{-1}{\cdot}mol^{-1}$) (6, 27) at its $T_{g,1} = 136 \pm 2$ K is much lower than the heat capacity increase for an HDA sample at 1 GPa and 140 K, which Andersson reported to be 3.2 $JK^{-1}{\cdot}mol^{-1}$ (13). This value is similar to $\Delta c_{p,2}$ as obtained here for HDA at ambient pressure. This suggests that the transition detected near 1 GPa (13) is thermodynamically connected to the one identified here near $T_{g,2}$, in accord with the double T_g scenario outlined in Fig. 1*B*. Conversely, this finding implies that LDA's ambient pressure glass transition (4–6) and the glass transitions observed at high pressures (12–15) are distinct phenomena, despite the similarity of the associated T_gs. The observation of two distinct glass transitions, $T_{g,1}$ and $T_{g,2}$, at ambient pressure rules out the possibility of a single T_g scenario sketched in Fig. 1*A*.

We emphasize that the repeatable endothermic effect observed here cannot be caused by annealing of microcracks or other effects that involve restructuring of the HDA surface. All these processes are related to a lowering of free energy and known to produce exotherms, but not endotherms in calorimetry. Furthermore, such processes take place only once, but not repeatedly in heating–cooling cycles. The endotherm is observed both for finely powdered eHDA samples and for large, single chunks of eHDA. The second glass transition is therefore clearly a bulk effect. Regarding the nature of water's second glass transition, it may be conceived that either the oxygen atoms, and thus complete water molecules, become mobile or that, alternatively, the oxygen atoms remain immobile, and only hydrogen atom mobility sets in upon heating above $T_{g,2}$. The former option implies translational motion of entire water molecules, decrease of viscosity, as well as sample softening and is called "glass-to-liquid transition." The latter option features only reorientational motion of water molecules (or H atoms jumping along a hydrogen bridge), is called "orientational" glass transition (28), and does not involve significant sample softening. Onset of hydrogen mobility alone, and thus an orientational glass transition, was observed in high-pressure crystalline ices such as ice IV, V, and XII (29). The associated thawing of hydrogen atom mobility, showing up between ~130 and 140 K, takes place on an H-bond network fulfilling the Bernal–Fowler ice rules and generates an increase in heat capacity of ~1 $JK^{-1}{\cdot}mol^{-1}$. The increase in heat capacity observed here near 116 K is about five times as large—direct evidence that the motion giving rise to the endotherms reported in Fig. 2 does not refer to an orientational glass transition, but indeed to a glass-to-liquid softening. By contrast, the increase in heat capacity when heating LDA beyond 136 K is similar to the one observed in high-pressure crystalline ices at the orientational glass transition. This suggests that by heating HDA near 116 K it enters a state that properly should be named high-density liquid (HDL). The use of this term will be further substantiated via the dielectric measurements to be presented in the following.

Dielectric Measurements. To probe relaxational properties of ultraviscous water, dielectric spectroscopy is ideally suited, but it was rarely used. Specifically, broadband–dielectric spectroscopy has not been used before to study amorphous water. LDA was studied using this technique either at ambient pressure only for a few frequencies (30–32) or under high-pressure conditions (33). HDA has never been investigated dielectrically at ambient pressure, to our knowledge. However, an "ultraviscous liquid state" related to HDA was inferred from high-pressure dielectric data (34) (>0.15 GPa). At ambient pressure, a loss peak arising from the structural relaxation in HDL heretofore has not been accessible because the relatively unstable uHDA available to earlier studies transforms directly to LDA. Also, a peaked loss spectrum arising from structural relaxation in low-density liquid (LDL) has not been observed so far. In the present work we were able to record the response of HDL and LDL over a frequency range of about six decades (from 10^{-2} Hz to 10^{+4} Hz), which enabled the direct observation of loss peaks for several temperatures.

For our experiments we investigated the dielectric response of eHDA samples by first ramping a powder sample from 77 K to 109 K, a temperature at which only the high-frequency part of a dielectric loss peak showing a pronounced excess wing is monitored (cf. Fig. 3*A*). Increasing the temperature successively to 124 K, the spectra shift to higher frequencies and loss peaks becomes fully resolved. Then, at 126 K, a "noisy" spectrum was

recorded demonstrating that the sample's change of state was caught in the act. The crosses in Fig. 3*A* indicate that at 128 K the loss peak has shifted to lower frequencies. The observation made at 126 K can thus be ascribed to a transformation from HDL to the low-density phase. The transformation temperature is slightly lower than in our calorimetry scans because of the much lower heating rates used for the dielectric experiments. Upon further heating, LDL loss patterns were acquired, which again shift successively to higher frequencies until just above 151 K, when another displacement to lower frequencies occurs, this time referring to the transformation from LDL to cubic ice (stars in Fig. 3*B*). The subsequent thermal history of our samples is indicated by the numbered green arrows in Fig. 4.

We determined time constants $\tau = 1/(2\pi\nu_m)$ from the loss peak frequencies ν_m and summarize the results as filled symbols in an Arrhenius diagram (Fig. 4). For temperatures at which a loss peak was not resolved, τ was assessed on the basis of time temperature superposition, a standard procedure applied when analyzing data for glass-forming liquids (crossed symbols in Fig. 4). The same procedure was applied for the results of additional samples for which a relaxation peak was not fully resolved. Fig. 4 demonstrates that the ice I_c, LDL, and HDL phases are clearly distinguishable solely on the basis of their relaxation time traces. Near their respective transformation temperatures, LDL relaxes about two decades faster than cubic ice, and HDL relaxes about two decades faster than LDL.

Based upon high-pressure data, Johari and Andersson rationalized the longer dielectric relaxation time of "LDA" relative to that of "HDA" by "a hydrogen bond structure in LDA, in which the ice rules are obeyed," whereas they state that "HDA may appear to be a densified state of water in which ice rules are not obeyed" (35). According to neutron diffraction studies, however, the local ordering in HDA satisfies the ice rules perfectly, even though an interstitial molecule, which itself obeys these rules, penetrates from the second into the first coordination shell (36). However, the interstitial water molecule forces the O–O distance to increase from 2.77 Å in LDA to 2.82 Å in HDA despite a ~25% higher density of the latter ("density–distance paradoxon")

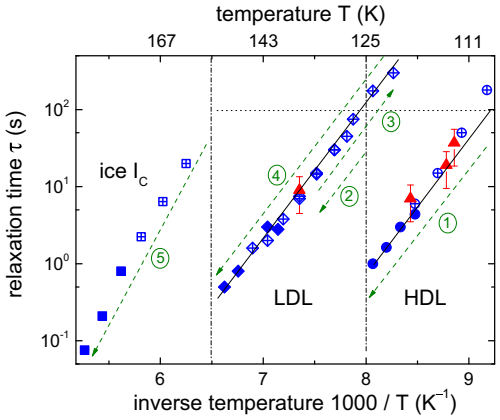

Fig. 4. Relaxation map of H_2O phases obtained from eHDA. Blue circles, diamonds, and squares refer to dielectric measurements. The numbered green arrows indicate the thermal history of our samples—that is, the temperature program used. The filled symbols were determined directly from peak frequencies, while the crossed symbols were obtained by applying time temperature superposition. The dash-dotted lines correspond to temperatures at which transitions occur; the dotted line marks a time scale of 100 s, which is usually associated with the glass transition temperature. Red triangles correspond to the calorimetric relaxation times τ_{cal}, calculated using Eq. **1**, for heating rates of q = 5, 10, and 30 K/min, which agree excellently with the dielectric time constants.

(37), which may explain the shorter dielectric relaxation times in HDL compared with those of LDL.

The dielectric relaxation times of LDL indicate thermal activation according to $\tau = \tau_0 \exp(\Delta E/k_B T)$ (see the well-fitting straight solid line in Fig. 4), with an activation energy of $\Delta E = 34 \pm 1$ kJ/mol and a preexponential factor $\tau_0 = 1 \times 10^{-12}$ s. In terms of the strong–fragile classification of glass formers (38), Novikov and Sokolov rationalize this very low fragility index in terms of quantum effects at T_g (39). LDL exhibits a kinetic fragility index of $m_1 = 14 \pm 1$ and is thus one of the strongest liquids known. With ΔE given, a calorimetric time scale (40)

$$\tau_{cal} = k_B T_g^2/(q\ \Delta E) \qquad [1]$$

can be calculated from our calorimetric data. In Fig. 4 the resulting τ_{cal} is seen to agree excellently with the dielectric relaxation times. Even if the uncertainty in ΔE were as large as ±50%, this only results in the modest "error bar" given in Fig. 4. Furthermore, for LDL we find that $T(\tau = 100s)$ is about 126 K, consistent with a 10 K/h scanning rate calorimetric study (27). In separate runs we checked whether the dielectric spectra yielding relaxation times $\tau > 100$ s reflect equilibrium measurements. To this end, the dielectric loss at the corresponding temperatures was monitored for more than 2 h and found to be invariant, demonstrating that equilibrium was always attained. As indicated by the sequence of arrows depicted in Fig. 4, the long-time measurements on the LDL sample were taken by cycling it to below 126 K.

Inspecting now, in Fig. 4, the relaxation times for HDL at ambient pressure, slight deviations between the solid line (again representing ΔE = 34 kJ/mol) and the experimental data are noted at low temperatures. Despite the fact that only slightly more than two decades in relaxation time could be covered for HDL, our finding suggests that this state of H_2O exhibits slight deviations from Arrhenius behavior. A rough estimate based on the relaxation times recorded near $T(\tau = 100s) \sim 110$ K yields a fragility index m_2 of about 20–25, but certainly not exceeding 40, a variously suggested value (11). Determining τ_{cal} from heating-rate–dependent DSC measurements as outlined above (cf. Eq. **1**) for HDL and using the same ΔE, we again obtain excellent agreement with the dielectric data (Fig. 4). We emphasize that the difference between the calorimetric glass transition temperature of 116 K and the dielectric glass transition temperature of 110 K is associated with the different heating rates used to study the samples. Although heating rates of 10 K/min are used in the case of DSC scans, the heating rates are much lower in the case of our dielectric study.

Orientational Glass Transition or Glass-to-Liquid Transition? To further clarify the nature of the glass transition in HDA, we investigated ice V near its orientational glass transition temperature, which calorimetrically shows up at ~138 K (29). We emphasize that the local order and packing in HDA is not very different from high-pressure ice phases such as ice V (41). We observe that $\Delta c_{p,2}$ of HDA at its $T_{g,2}$ (trace 3 of Fig. 2) is five times larger than Δc_p of ice V at its T_g (42, 43). For ice V, Δc_p reflects solely the thawing of orientational degrees of freedom. However, for HDA, contributions stemming from translational motions are required to explain its large $\Delta c_{p,2}$. Thus, the notion of an orientational glass transition, at which hydrogen atom motions govern the entropy change, cannot be reconciled with the observed magnitude of $\Delta c_{p,2}$. The latter obviously reflects the unfreezing also of translational motion of oxygen atoms, indicative of an underlying glass-to-liquid transition in HDA.

In the context of the strong–fragile classification (38), it is instructive to compare the spectral shapes of the dielectric loss curves of HDL and LDL with each other as well as with results

on glycerol, an archetypical glass-forming liquid. Fig. 3*A* reveals that the loss pattern of HDL is similar to that of supercooled glycerol (dashed curve) (44), both exhibiting a pronounced excess wing. [Brand et al. (45) state that "except for cyclo-hexanol, in all plastic crystals investigated so far there is compelling evidence against the presence of an excess wing in its original sense." This statement still reflects the state-of-the-art with the added comment that even in cyclo-octanol the excess wing has a much smaller amplitude than in conventional glass formers. Hence, the observation of a pronounced wing-like feature in the dielectric spectra of HDL is a strong hint that HDL is indeed a supercooled liquid and not a plastic crystal.] For LDL, the high-frequency flank of the dielectric loss is a factor of ∼1.4 steeper, indicating its less stretched and hence more exponential dielectric response. In addition, LDL exhibits a low-loss, high-frequency feature that is reminiscent of a secondary relaxation, in agreement with earlier temperature-dependent measurements carried out at 1 and 10 kHz (31, 32). Thus, the interpretation as HDL is in accord with high-pressure work, in which the data have been interpreted in favor of the existence of HDL (12–15, 34, 46). The larger kinetic fragility of HDL compared with that of LDL is in harmony with our DSC results. HDL's larger Δc_p is consistent with it being a "less strong" glass former than LDL, one of the "strongest" glass formers known so far. We do not call HDL a "fragile" liquid, as those show fragility indices m of about 80 or more (38) and heat capacity steps on the order of 100 $JK^{-1}{\cdot}mol^{-1}$, which compares to ∼5 $JK^{-1}{\cdot}mol^{-1}$ for HDL and ∼1 $JK^{-1}{\cdot}mol^{-1}$ for LDL.

Discussion

Let us finally turn to the implications for our understanding of the phase behavior of metastable water. We here observe several phase transformations by heating eHDA at ambient pressure. Overall, the sample transforms in steps from a highly metastable phase to less and less metastable phases and finally reaches a thermodynamically stable phase according to the sequence HDL→LDL→cubic ice→hexagonal ice. The transformation from the high-density to the low-density phase observed here at ambient pressure does not involve equality of Gibbs free energies (17). The Gibbs free energies of low-density and high-density phases are considered to be equal only at high-pressure conditions, typically at about 0.2 GPa (47). This sequence of transformations at ambient pressure is similar to the previously known sequence of transformations of uHDA (20, 48). However, what is different is that eHDA—a more relaxed HDA form than uHDA—has a higher thermal stability and consequently transforms to the low-density phase at higher temperature. The additional temperature window accessible to the high-density phase allows for the structural and dielectric relaxation times to drop far enough so that values lower than 100 s can be accessed without transformation to the low-density phase above $T_{g,2}$, which corresponds to a liquid-like situation. Circumstantial evidence for HDL—that is, for the liquid (rather than solid) nature of the high-density sample above $T_{g,2}$—is provided by the difference in activation energy between solid ice V above its orientational glass transition (81 ± 6 kJ/mol) and eHDA above $T_{g,2}$ (34 ± 1 kJ/mol) and by the magnitude of the heat capacity increase at $T_{g,2}$, which is much more than the increase in heat capacity expected for an orientational glass transition at T_g involving mobility of hydrogen, but not of oxygen atoms.

At ambient pressure, HDL slowly converts with time to the low-density phase, but can be kept for many hours—for example, at 120 K. Similarly, LDL can be kept—for example, at 140 K—and converts only very slowly to cubic ice. The transformation to the low-density phase may be related to spinodal decomposition of HDL at 1 bar above 132 K, which would imply that the HDL spinodal crosses the ambient pressure axis at low temperature. In many simulation studies, such low temperatures are not considered and so it is unclear which of the water models describe the experimentally observed transformation sequence. As pointed out by Giovambattista et al., the high- to low-density conversion may be a "result of HDA reaching its T_g, rather than being associated with the HDL-to-LDL spinodal" (17). In our calorimetric experiments, HDA reaches its $T_{g,2}$ and, thus, the HDL state at 116 K and then releases latent heat at 132 K at a 10 K/min heating rate, which is associated with the sudden transformation to the low-density phase. From these experiments we cannot say with certainty whether this transformation reflects a spinodal decomposition. Overall, our findings represent benchmark data for further improvement of contemporary water models and pave the way for a wide range of experimental studies aimed at more detailed characterizations of water's second deeply supercooled liquid state. In particular, all methods that are restricted to a (sub)ambient pressure sample environment are now feasible for investigation of HDL's properties.

The main experimental finding of the present work is the observation of two distinct glass transitions at ambient pressure, an observation ruling out a connection of water's "old" ambient-pressure glass transition at $T_{g,1}$ ∼ 136 K with the recently reported high-pressure glass transitions of water (12–15). That is, the single T_g scenario in Fig. 1*A* does not describe water. Instead, we suggest that the here-reported $T_{g,2}$ at ambient pressure connects with the high-pressure glass transition, whereas the liquid emanating from LDA is thermodynamically not continuously connected with high-pressure water, in accord with the double T_g scenario depicted in Fig. 1*B* and with simulations of the ST2 water model, but not of the SPC/E model (17). Just like in our experiments, ST2 water shows the low-pressure glass transition of HDA also to be at lower temperatures than the low-pressure glass transition of LDA (see figure 3c in ref. 17). Our experimental indications for both HDL and LDL support two-liquid interpretations of supercooled water, but do not directly address the question of whether there is a first-order liquid–liquid transition ending in a liquid–liquid critical point (49) or whether HDL and LDL can transform into each other in a singularity-free scenario (50). This is because we observe these liquids at temperatures below the "no man's land," far from the purported critical point (16), and at ambient pressure, far from the equilibrium transformation boundary (51). However, our study reveals that both HDL and LDL can be observed experimentally, and in terms of fragility, the transformation from HDL to LDL involves a dynamic crossover from a less strong to a very strong liquid. This finding settles a long-standing question in understanding water, in which LDL near 140 K was postulated to be "strong" (8, 52–55), "not strong" (56), "not fragile" (9, 11, 57), or "the strongest liquid yet identified" (58). In fact, our temperature-dependent dielectric and heating-rate–dependent calorimetric data classify LDL as a "superstrong" liquid (59), which shows the lowest steepness index $m_1 = 14 \pm 1$ of all liquids. Also, HDL near 120 K falls into the category of strong liquids, albeit the steepness index m_2 = 20–25 makes it less strong than LDL. That is, neither LDL nor HDL are fragile liquids in the deeply supercooled, ultraviscous state. The $T_{g,2} = 116 \pm 2$ K revealed in this study represents the lowest temperature, above which liquid-like translational mobility of bulk water has been inferred from laboratory experiments, and so one may speculate that well-annealed astrophysical ices may be encountered in this deeply supercooled liquid-like state even at such low temperatures—for example, subsurface ices on icy moons.

Materials and Methods

The samples studied in this work were prepared and characterized in Innsbruck and transferred to Dortmund under liquid nitrogen conditions. eHDA samples were prepared according to Winkel et al. (21). Similar to our previous work (24), eHDA samples have been confirmed by powder X-ray diffraction to be free from contamination by other ice phases and by FTIR spectroscopy

to be free from chemical impurities. For the DSC measurements, we powdered the eHDA samples, transferred the powder under liquid nitrogen into crucibles, and cold-loaded the crucibles at ~90 K into the instrument. Aluminum crucibles were used for measurements in a Perkin–Elmer DSC8000 (Fig. 2) and steel crucibles for measurements in a Perkin–Elmer DSC4e (Fig. 2, *Inset*). For dielectric measurements, we transferred the powder into a parallel plate capacitor while keeping the temperature always below 100 K, and investigated their dielectric response using an Alpha Analyzer from Novocontrol. Due to the uncertainty in estimating the cells' exact filling factor, the dielectric loss is given in arbitrary units. The samples were investigated by heating them in steps of 3 K using a heating ramp of 0.5 K/min between successive frequency scans. During the acquisition of each spectrum, requiring ~10 min, the temperature was stabilized to within 0.1 K. Taking into account also waiting times between frequency scans, the overall heating rates are about 0.01 K/min near the transition to LDA and about 0.02 K/min near the transition to cubic ice.

ACKNOWLEDGMENTS. We thank Chae Un Kim for discussion, Marion Bauer for carefully calibrating the DSC instrument, and the European Research Council (Starting Grant SULIWA), the Austrian Science Fund FWF (Firnberg Award T463 to K.A.-W. and START Award Y394 to T.L.), and the Austrian Academy of Sciences (ÖAW, DOC fellowship to M.S.) for financial support.

1. Klinger J (1985) Amorphous ice in astrophysics. *J Phys Colloq* 46(C8):657–660.
2. Mayer E, Pletzer R (1985) *Ices in the Solar System*, eds Klinger J, Benest D, Dollfus A, Smoluchowski R (D. Reidel Publishing Company, Dordrecht, The Netherlands), pp 81–88.
3. Jenniskens P, Blake DF, Wilson MA, Pohorille A (1995) High-density amorphous ice, the frost on interstellar grains. *Astrophys J* 455(1):389–401.
4. McMillan JA, Los SC (1965) Vitreous ice: Irreversible transformations during warm-up. *Nature* 206(4986):806–807.
5. Johari GP, Hallbrucker A, Mayer E (1987) The glass-liquid transition of hyperquenched water. *Nature* 330(6148):552–553.
6. Elsaesser MS, Winkel K, Mayer E, Loerting T (2010) Reversibility and isotope effect of the calorimetric glass → liquid transition of low-density amorphous ice. *Phys Chem Chem Phys* 12(3):708–712.
7. Velikov V, Borick S, Angell CA (2001) The glass transition of water, based on hyperquenching experiments. *Science* 294(5550):2335–2338.
8. Kohl I, Bachmann L, Mayer E, Hallbrucker A, Loerting T (2005) Water behaviour: Glass transition in hyperquenched water? *Nature* 435(7041):E1–E2, discussion E1–E2.
9. McClure SM, Safarik DJ, Truskett TM, Mullins CB (2006) Evidence that amorphous water below 160 K is not a fragile liquid. *J Phys Chem B* 110(23):11033–11036.
10. Angell CA (2008) Insights into phases of liquid water from study of its unusual glass-forming properties. *Science* 319(5863):582–587.
11. Capaccioli S, Ngai KL (2011) Resolving the controversy on the glass transition temperature of water? *J Chem Phys* 135(10):104504.
12. Mishima O (2004) The glass-to-liquid transition of the emulsified high-density amorphous ice made by pressure-induced amorphization. *J Chem Phys* 121(7): 3161–3164.
13. Andersson O (2011) Glass-liquid transition of water at high pressure. *Proc Natl Acad Sci USA* 108(27):11013–11016.
14. Seidl M, et al. (2011) Volumetric study consistent with a glass-to-liquid transition in amorphous ices under pressure. *Phys Rev B* 83(10):100201.
15. Handle PH, Seidl M, Loerting T (2012) Relaxation time of high-density amorphous ice. *Phys Rev Lett* 108(22):225901.
16. Poole PH, Sciortino F, Essmann U, Stanley HE (1992) Phase behavior of supercooled water. *Nature* 360(6402):324–328.
17. Giovambattista N, Loerting T, Lukanov BR, Starr FW (2012) Interplay of the glass transition and the liquid-liquid phase transition in water. *Scientific Rep* 2:390.
18. Debenedetti PG (2003) Supercooled and glassy water. *J Phys Condens Matter* 15(45): R1669–R1726.
19. Loerting T, et al. (2011) How many amorphous ices are there? *Phys Chem Chem Phys* 13(19):8783–8794.
20. Handa YP, Mishima O, Whalley E (1986) High-density amorphous ice. III. Thermal properties. *J Chem Phys* 84(5):2766–2770.
21. Winkel K, Mayer E, Loerting T (2011) Equilibrated high-density amorphous ice and its first-order transition to the low-density form. *J Phys Chem B* 115(48):14141–14148.
22. Jenniskens P, Blake DF (1994) Structural transitions in amorphous water ice and astrophysical implications. *Science* 265(5173):753–756.
23. Nelmes RJ, et al. (2006) Annealed high-density amorphous ice under pressure. *Nat Phys* 2(6):414–418.
24. Winkel K, Elsaesser MS, Mayer E, Loerting T (2008) Water polyamorphism: Reversibility and (dis)continuity. *J Chem Phys* 128(4):044510.
25. Mishima O, Calvert LD, Whalley E (1984) "Melting ice" I at 77 K and 10 kbar: A new method of making amorphous solids. *Nature* 310(5976):393–395.
26. Angell CA (2004) Amorphous water. *Annu Rev Phys Chem* 55:559–583.
27. Handa YP, Klug DD (1988) Heat capacity and glass transition behavior of amorphous ice. *J Phys Chem* 92(12):3323–3325.
28. Fisher M, Devlin JP (1995) Defect activity in amorphous ice from isotopic exchange data: Insight into the glass transition. *J Phys Chem* 99(29):11584–11590.
29. Salzmann CG, Radaelli PG, Slater B, Finney JL (2011) The polymorphism of ice: Five unresolved questions. *Phys Chem Chem Phys* 13(41):18468–18480.
30. Koverda VP, Bogdanov NM, Skripov VP (1983) Self-sustaining crystallization of amorphous layers of water and heavy water. *J Non-Cryst Solids* 57(2):203–212.
31. Johari GP, Hallbrucker A, Mayer E (1991) The dielectric behavior of vapor-deposited amorphous solid water and of its crystalline forms. *J Chem Phys* 95(4):2955–2964.
32. Johari GP, Hallbrucker A, Mayer E (1992) Dielectric study of the structure of hyperquenched glassy water and its crystallized forms. *J Chem Phys* 97(8):5851–5855.
33. Andersson O (2007) Dielectric relaxation of low-density amorphous ice under pressure. *Phys Rev Lett* 98(5):057602.
34. Andersson O, Inaba A (2006) Dielectric properties of high-density amorphous ice under pressure. *Phys Rev B* 74(18):184201.
35. Johari GP, Andersson O (2007) Vibrational and relaxational properties of crystalline and amorphous ices. *Thermochim Acta* 461(1-2):14–43.
36. Finney JL, Hallbrucker A, Kohl I, Soper AK, Bowron DT (2002) Structures of high and low density amorphous ice by neutron diffraction. *Phys Rev Lett* 88(22):225503.
37. Loerting T, Salzmann C, Kohl I, Mayer E, Hallbrucker A (2001) A second distinct structural "state" of high-density amorphous ice at 77 K and 1 bar. *Phys Chem Chem Phys* 3(24):5355–5357.
38. Böhmer R, Ngai KL, Angell CA, Plazek DJ (1993) Nonexponential relaxations in strong and fragile glass formers. *J Chem Phys* 99(5):4201–4209.
39. Novikov VN, Sokolov AP (2013) Role of quantum effects in the glass transition. *Phys Rev Lett* 110(6):065701.
40. Hodge IM (1994) Enthalpy relaxation and recovery in amorphous materials. *J Non-Cryst Solids* 169(3):211–266.
41. Saitta AM, et al. (2004) High density amorphous ices: Disordered water towards close packing. *J Chem Phys* 121(17):8430–8434.
42. Salzmann CG, Kohl I, Loerting T, Mayer E, Hallbrucker A (2003) The low-temperature dynamics of recovered ice XII as studied by differential scanning calorimetry: A comparison with ice V. *Phys Chem Chem Phys* 5(16):3507–3517.
43. Salzmann CG, Radaelli PG, Finney JL, Mayer E (2008) A calorimetric study on the low temperature dynamics of doped ice V and its reversible phase transition to hydrogen ordered ice XIII. *Phys Chem Chem Phys* 10(41):6313–6324.
44. Kudlik A, Benkhof S, Blochowicz T, Tschirwitz C, Rössler E (1999) The dielectric response of simple organic glass formers. *J Mol Struct* 479(2-3):201–218.
45. Brand R, Lunkenheimer P, Loidl A (2002) Relaxation dynamics in plastic crystals. *J Chem Phys* 116(23):10386–10401.
46. Mishima O, Suzuki Y (2001) Vitrification of emulsified liquid water under pressure. *J Chem Phys* 115(9):4199–4202.
47. Whalley E, Klug DD, Handa YP (1989) Entropy of amorphous ice. *Nature* 342(6251): 782–783.
48. Mishima O, Calvert LD, Whalley E (1985) An apparently first order transition between two amorphous phases of ice induced by pressure. *Nature* 314(6006):76–78.
49. Poole PH, Sciortino F, Essmann U, Stanley HE (1992) Phase behavior of metastable water. *Nature* 360(6402):324–328.
50. Sastry S, Debenedetti PG, Sciortino F, Stanley HE (1996) Singularity-free interpretation of the thermodynamics of supercooled water. *Phys Rev E* 53(6):6144–6154.
51. Mishima O (1994) Reversible first-order transition between two H2O amorphs at apprx. 0.2 GPa and apprx. 135 K. *J Chem Phys* 100(8):5910–5912.
52. Angell CA (1993) Water-II is a strong liquid. *J Phys Chem* 97(24):6339–6341.
53. Jenniskens P, Blake DF (1996) Crystallization of amorphous water ice in the Solar System. *Astrophy J* 473(2, Pt. 1):1104–1113, 1 plate.
54. Tanaka H (2003) A new scenario of the apparent fragile-to-strong transition in tetrahedral liquids: Water as an example. *J Phys Condens Matter* 15(45):L703–L711.
55. Kohl I, Bachmann L, Hallbrucker A, Mayer E, Loerting T (2005) Liquid-like relaxation in hyperquenched water at < or = 140 K. *Phys Chem Chem Phys* 7(17):3210–3220.
56. Mayer E, Hallbrucker A, Sartor G, Johari GP (1995) Glass-liquid transition and devitrification of $LiCl.11H_2O$ solution and of hyperquenched and vapor-deposited water. *J Phys Chem* 99(14):5161–5165.
57. Minoguchi A, Richert R, Angell CA (2004) Dielectric studies deny existence of ultraviscous fragile water. *Phys Rev Lett* 93(21):215703.
58. Ito K, Moynihan CT, Angell CA (1999) Thermodynamic determination of fragility in liquids and a fragile-to-strong liquid transition in water. *Nature* 398(6727):492–495.
59. Angell CA, Moynihan CT, Hemmati M (2000) 'Strong' and 'superstrong' liquids, and an approach to the perfect glass state via phase transition. *J Non-Cryst Solids* 274(1-3): 319–331.